TOPICAL REVIEW

Time-resolved and continuous-wave optical spin pumping of semiconductor quantum wells

G. V. Astakhov[1,2], M. M. Glazov[2], D. R. Yakovlev[2,3], E. A. Zhukov[3,4], W. Ossau[1], L. W. Molenkamp[1], and M. Bayer[3]

[1]Physikalisches Institut (EP3), Universität Würzburg, D-97074 Würzburg, Germany
[2]A.F. Ioffe Physico-Technical Institute, Russian Academy of Sciences, 194021 St. Petersburg, Russia
[3]Experimentelle Physik 2, Technische Universität Dortmund, D-44221 Dortmund, Germany
[4]Faculty of Physics, M.V. Lomonosov Moscow State University, 119992 Moscow, Russia

Abstract.

Experimental and theoretical studies of all-optical spin pump and probe of resident electrons in CdTe/(Cd,Mg)Te semiconductor quantum wells are reported. A two-color Hanle-MOKE technique (based on continuous-wave excitation) and time-resolved Kerr rotation in the regime of resonant spin amplification (based on pulsed excitation) provide a complementary measure of electron spin relaxation time. Influence of electron localization on long-lived spin coherence is examined by means of spectral and temperature dependencies. Various scenarios of spin polarization generation (via the trion and exciton states) are analyzed and difference between continuous-wave and pulsed excitations is considered. Effects related to inhomogeneous distribution of g-factor and anisotropic spin relaxation time on measured quantities are discussed.

1. Introduction

Optical spin pumping of resident electrons in bulk semiconductors has been established since the seventies of the past century [1]. The circularly polarized light induces interband transitions between the hole states in the valence band (VB) and the electron states (e) in the conduction band (CB). Owing to the optical selection rules the allowed photo-generated electron-hole pairs in the case of σ^+ excitation are $(hh, +3/2; e, -1/2)$ and $(lh, +1/2; e, +1/2)$. Here, $(hh, \pm 3/2)$ denotes the heavy-hole state with spin projection $j_z = \pm 3/2$ on the incident direction of the light, $(lh, \pm 1/2)$ denotes the light-hole state with $j_z = \pm 1/2$ and $(e, \pm 1/2)$ the electron state with $s_z = \pm 1/2$. Since the matrix elements of the heavy-hole and light-hole transitions relate as $\sqrt{3}$ to 1, σ^+ excitation creates predominantly spin-down electrons, i.e., with $s_z = -1/2$ (Fig. 1). If hole spin flip occurs, the hole can recombine with a spin-up electron emitting σ^--polarized photon. As a result, the total electron spin $S_z = (n_+ - n_-)/2$ after recombination is not zero any more ($n_\pm$ is concentration of $s_z = \pm 1/2$ electrons). The net spin polarization is equal

$$\rho_e = 2S_z/n_e\,, \tag{1}$$

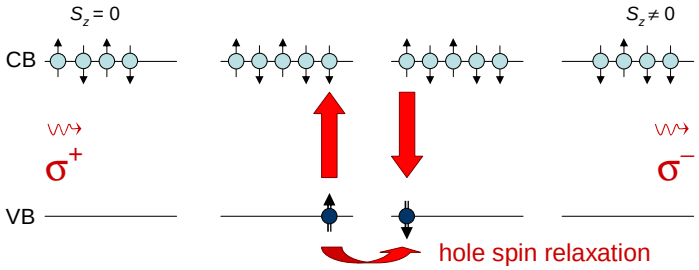

Figure 1. Schematic illustration of the optical spin pumping of resident electrons in bulk semiconductors. Wavy lines show incident σ^+ and emitted σ^- photons. Arrows $\uparrow$ ($\downarrow$) correspond to the electrons with $s_z = +1/2$ ($s_z = -1/2$). Arrows $\Uparrow$ ($\Downarrow$) correspond to the heavy-holes with $j_z = +3/2$ ($j_z = -3/2$). S_z denotes the total electron spin of electrons.

where n_e is the total electron concentration. Typically, a hole looses its spin quickly and the electron spin relaxation time τ_s is rather long. As a consequence, the optically created electron spins are accumulated in $s_z = -1/2$ state under continuous wave (cw) excitation with σ^+ polarization. This implies optical spin pumping. The theoretical limit of the steady-state net spin polarization is $\rho_e = 0.5$ [1]. This is valid for bulk semiconductors with degenerated light-hole and heavy-hole states, like GaAs and CdTe.

In bulk n-type semiconductors the circular polarization degree of the edge photoluminescence (PL) $P = (I_+^+ - I_+^-)/(I_+^+ + I_+^-)$ is proportional to the net spin polarization $P = \rho_e/2$. Here, $I_+^\pm$ is the PL intensity of the corresponding optical transition under $\sigma^\pm$ excitation detected in σ^+-polarization component. When an in-plane magnetic field B is applied electron spins start to precess around magnetic field direction with the Larmor frequency $\omega_L = g_e \mu_B B/\hbar$, where g_e is electron g-factor and μ_B is the Bohr magneton. As a result, S_z decreases following

$$S_z(B) = \frac{S_z(0)}{1 + (B/B_{1/2})^2}. \tag{2}$$

Such a behavior detected by means of the PL circular polarization $P \propto S_z$ is known as the Hanle effect [1]. The average electron spin drops by a factor of 2 when the electron spin lifetime T_s and the Larmor frequency ω_L satisfy the condition $\omega_L T_s = 1$. This condition defines characteristic magnetic field $B_{1/2} = \hbar/(\mu_B g_e T_s)$ allowing to obtain T_s if g-factor is known. These experiments can be performed under cw optical excitation.

In n-type semiconductors an additional spin decay channel is the recombination of resident electrons with photogenerated holes. As a consequence the spin lifetime depends on pump density W as

$$T_s^{-1} = \tau_s^{-1}(1 + W/W_0)\,. \tag{3}$$

Using Eq. (2) in the limit of low excitation density (i.e., W much below the characteristic pump density W_0) one can find the spin relaxation time of 'unperturbed' electron system τ_s, as $T_s \to \tau_s$.

Time resolved spectroscopy based on pulsed photoexcitation offers straightforward access to the carrier spin dynamics (for overview see Ref. [2]). For example, polarized photoluminescence measured by streak-camera allows to follow spin relaxation during the exciton lifetime. Faraday and Kerr rotation techniques can monitor

magnetization induced by spin polarized carriers at time delays not limited by exciton recombination. In external magnetic fields not only spin dynamics but also Zeeman splitting for carriers and excitons can be measured from the period of signal oscillations. Respectively, the direct evaluation of carrier and exciton g-factors became possible. Partial limitations of time-resolved techniques are related to relatively high peak density of photoexcitation as compared to cw excitation. This may cause perturbation of electronic system (carrier heating, nonequilibrium distribution) which can affect the spin dynamics.

In low-dimensional quantum well (QW) heterostructures the optical spin pumping can be modified due to following reasons. (i) Quantum confinement and strain lift up the degeneracy of light-hole and heavy-hole states. Hence, their selective excitation becomes possible and theoretical limit for the net spin polarization in this case is increased to 100% ($|\rho_e| = 1$). (ii) In n-type modulation doped QWs a negatively charged trion (T) becomes stable. It is composed of a hole and two electrons, the latter form the spin singlet [3]. The singlet state itself does not contribute to the spin polarization, but resonant excitation of trions and/or trion formation from excitons provide an efficient mechanism for polarization of resident electrons in QWs [4].

The goal of this paper is to perform a comparative study of electron spin dynamics under cw and pulsed photoexcitation and to clarify whether the same values of spin relaxation times can be achieved by both techniques. Experiments are done for the very same samples, which are CdTe/(Cd,Mg)Te quantum well structures with diluted concentration of resident electrons.

The paper is organized as follows. We start with model considerations of the generation of spin polarization and spin coherence in quantum wells with diluted two-dimensional electron gas. Then we present experimental results for cw and pulsed excitation, analyze them and conclude.

2. Theory

In the present section different scenarios of spin polarization generation and spin dynamics in transverse magnetic field are discussed. We consider both continuous wave (cw) and pulsed excitation regimes and we discuss one after another the mechanisms of spin pumping under excitation at the trion and exciton resonances.

2.1. Spin coherence excitation

Here we analyze the processes responsible for the generation of the electron spin coherence in QWs with low density two-dimensional electron gas (2DEG). It is assumed that the temperature measured in energy units k_BT is smaller than both exciton and trion binding energies and that the resident electron concentration is so small that trion and exciton states are stable (i.e. these states are not screened by electron-electron interactions). More detailed analysis is published in [4].

2.1.1. Trion resonant pumping

Continuous wave excitation. First, we consider the case where the trion is resonantly excited. The trion ground state forms the singlet spin structure, i.e., the spins of the two electrons involved in the trion are oriented antiparallel [5, 6]. A σ^+ polarized photon creates an electron-hole pair $(hh, +3/2; e, -1/2)$ and simultaneously

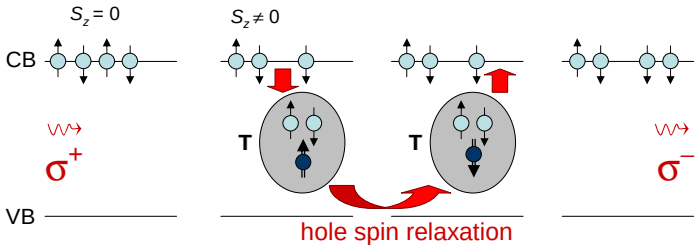

Figure 2. Schematic illustration of the optical spin pumping of resident electrons in QWs, resonant excitation to the trion (T).

an electron with the spin projection $s_z = +1/2$ is picked out from the resident ensemble in order to form a trion (Fig. 2). Thus, the resident ensemble becomes depleted of electrons with the spin projection opposite to that of photocreated ones, i.e. in our case the number of spin $s_z = +1/2$ electrons decreases. This means that a spin polarization of resident carriers $S_z \neq 0$ appears. The electrons returning to the ensemble after trion recombination can compensate this polarization. However, if the hole spin relaxation time in the trion is much shorter than the trion radiative lifetime the returned electrons are spin unpolarized and the spin polarization generated at the moment of absorption is conserved.

From the considerations above it is clear that at the initial moment each absorbed $\sigma^{\pm}$ photon increases the spin of resident electrons by $\mp 1/2$. In order to study the pump power dependence of the spin polarization generation we use the system of coupled kinetic equations describing the populations of electrons with different spins $n_{\pm}$, and populations of singlet trions $T_{\pm}$ (with the heavy-hole spin $\pm 3/2$)

$$
\begin{aligned}
&-\frac{T_+}{\tau_0^T} - \frac{T_+}{2\tau_s^T} + \frac{T_-}{2\tau_s^T} + n_+ G = 0, \\
&-\frac{T_-}{\tau_0^T} - \frac{T_-}{2\tau_s^T} + \frac{T_+}{2\tau_s^T} = 0, \\
&-\frac{n_+}{2\tau_s} + \frac{n_-}{2\tau_s} + \frac{T_+}{\tau_0^T} - n_+ G = 0, \\
&-\frac{n_-}{2\tau_s} + \frac{n_-}{2\tau_s} + \frac{T_-}{\tau_0^T} = 0.
\end{aligned}
\tag{4}
$$

Here it is assumed that the pumping is σ^+ polarized, G is the generation rate (being proportional to the pump density W), τ_0^T is the trion radiative lifetime, τ_s^T is the spin relaxation time of a hole in a trion (trion spin relaxation time), and τ_s is the spin relaxation time of resident electrons. System (4) should be complemented with the condition

$$T_+ + T_- + n_+ + n_- = n_e,$$

which describes conservation of resident electrons n_e.

The total steady state spin of resident electrons can be written as

$$S_z = \frac{n_+ - n_-}{2} = -\frac{n_e}{2} \frac{G\tau_s}{2\tau_s^T/\tau^T + G\tau_0^T \tau_s^T/\tilde{\tau}}, \tag{5}$$

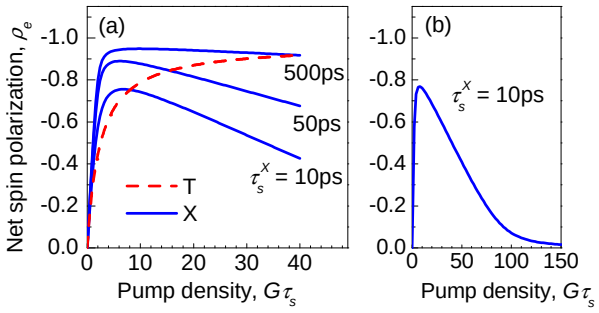

Figure 3. (a) Spin polarization of resident electrons ρ_e as a function of the generation rate in units of $G\tau_s$ under σ^+ excitation. Dashed curve corresponds to the trion resonant pumping. Solid curves correspond to the exciton resonant pumping. They are labeled by the respective electron-in-exciton spin relaxation time, τ_s^X. All curves are obtained for the electron spin relaxation time $\tau_s = 2$ ns, the exciton and trion radiative lifetimes $\tau_0^X = \tau_0^T = 50$ ps, the spin relaxation time of a hole in a trion $\tau_s^T = 10$ ps. The exciton to trion conversion coefficient is $\gamma n_e = 1$ ps. (b) The spin polarization of resident electrons (under the exciton resonant pumping) shown for a wide range of $G\tau_s$ ($\tau_s^X = 10$ ps).

where $\tau^T = \tau_s^T \tau_0^T/(\tau_s^T + \tau_0^T)$ is the trion spin lifetime including both the trion lifetime τ_0^T and the trion spin relaxation time τ_s^T, and

$$\frac{1}{\tilde{\tau}} = \frac{1}{\tau^T} + \frac{\tau_s}{\tau_s^T \tau_0^T}.$$

In experimental conditions [4] the electron spin relaxation time $\tau_s \gg \tau_0^T, \tau_s^T$. Therefore Eq. (5) can be recast as

$$S_z = \frac{n_+ - n_-}{2} = -\frac{n_e}{2} \frac{G\tau_s}{2\tau_s^T/\tau^T + G\tau_s}. \tag{6}$$

The net spin polarization $\rho_e = 2S_z/n_e$ is plotted as a function of $G\tau_s$ in Fig. 3(a) by the dashed line. The parameters of calculation are given in the figure caption.

At low pumping densities $G\tau_s \ll \tau_s^T/\tau^T$, i.e., where the spin polarization is small and no saturation effects are observed the electron spin grows linearly with the pumping density as

$$S_z = -\frac{n_e}{4} G \frac{\tau_s \tau^T}{\tau_s^T}. \tag{7}$$

It is worth noting that the absolute value of the electron spin $|S_z|$ decreases with an increase of trion spin relaxation time τ_s^T. It is in agreement with the qualitative picture outlined above: in order to induce the spin coherence of resident electrons the spin-flip of a hole in a trion is required. That means that τ_s^T should be comparable or shorter than the trion lifetime $\tau_0^T = 50$ ps. With further increase of the pump density the total spin of resident electrons grows sublinearly (Fig. 3). This is because the larger $|S_z|$ the less resident electrons with proper spin required to form the trion (i.e., $s_z = +1/2$) are left.

At high pump densities $G\tau_s \gg \tau_s^T/\tau^T$ the electron spin saturates at

$$S_z = -\frac{n_e}{2} \frac{\tau_s \tilde{\tau}}{\tau_0^T \tau_s^T} \approx -\frac{n_e}{2}. \tag{8}$$

This means that almost all resident electrons become spin polarized: $\rho_e \approx -1$. The negative sign results from the σ^+ pumping when electrons with spin $s_z = -1/2$ are created. The minority of electrons $s_z = +1/2$ are bound in trions whose density is $n_e(\tau_0^T + \tau_s^T)/\tau_s \ll n_e$. This implies that efficient spin pumping of resident electrons may be achieved at relatively low excitation densities. Such an unexpected behaviour is a direct consequence of the long spin relaxation of resident carriers. With increasing pump density the spin-up electrons ($s_z = +1/2$) are captured to the trions and return back unpolarized. The stronger pumping the less electrons have appropriate spin orientation and the number of trions decreases.

Pulsed excitation. Under pulsed excitation the physical processes governing electron polarization generation are essentially the same as for cw excitation [4]. After the trion formation the electron gas becomes depleted of electrons with the spin projection opposite to that of photocreated ones. The spin flip of a hole in a trion results in the imbalance of the spins of resident electrons and those returning after trion radiative recombination.

It is worth noting that the initial number of photogenerated trions under pulsed resonant excitation (n_0^T) cannot exceed $n_e/2$, where n_e is the density of resident electrons. Thus, the n_0^T increases linearly with the pump intensity for small excitation density and then saturates at the value $n_e/2$. The total generated electron spin at $\tau_0^T \gg \tau_s^T$ can be evaluated as

$$S_z = -\frac{n_e}{4} G\tau_0^T/(1 + G\tau_0^T), \tag{9}$$

where G is the generation rate being proportional to the pump power.

It is instructive to compare this result with the result of Eq. (8) obtained for the steady-state pumping. In the case of pulsed excitation the maximum total spin of resident electrons is $-n_e/4$, i.e., twice smaller than the steady-state value.

2.1.2. Exciton resonant pumping

Continuous wave excitation. Next, we discuss the case of exciton resonant pumping. Photocreated excitons can capture resident electrons and form trions. This process is schematically shown in Fig. 4. Under the assumption that the hole in the exciton looses its spin rapidly one may label concentrations of X_+ and X_- excitons in accordance with the electron spin projection in the exciton. The trions formed from these excitons are unpolarized because the spin of the paired electrons in the trion is zero and the hole spin is lost prior to trion formation. The kinetic equations describing such a situation write

$$\begin{aligned}
&-\frac{X_+}{\tau_0^X} - \frac{X_+}{2\tau_s^X} + \frac{X_-}{2\tau_s^X} - \gamma n_- X_+ = 0 \\
&-\frac{X_-}{\tau_0^X} - \frac{X_-}{2\tau_s^X} + \frac{X_+}{2\tau_s^X} - \gamma n_+ X_- + G_X = 0 \\
&-\frac{T}{\tau_0^T} + \gamma n_- X_+ + \gamma n_+ X_- = 0, \\
&-\frac{n_+}{2\tau_s} + \frac{n_-}{2\tau_s} + \frac{T}{2\tau_0^T} - \gamma n_+ X_- = 0, \\
&-\frac{n_-}{2\tau_s} + \frac{n_-}{2\tau_s} + \frac{T}{2\tau_0^T} - \gamma n_- X_+ = 0.
\end{aligned} \tag{10}$$

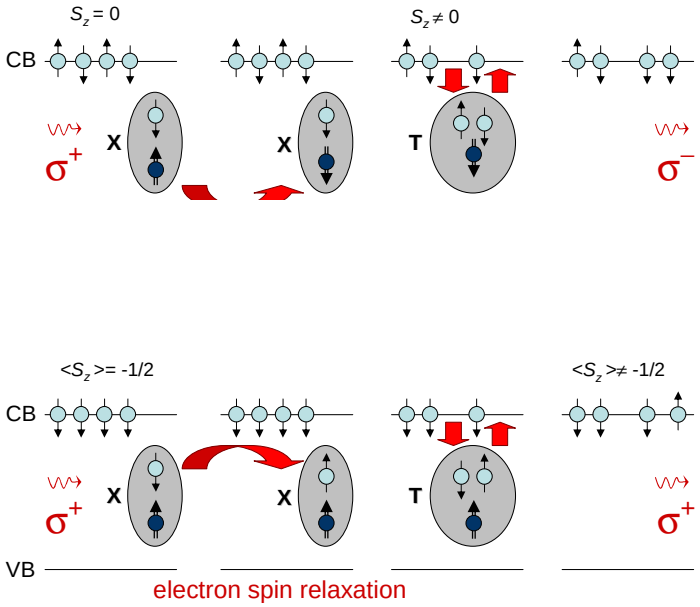

lent electrons
density.

Figure 5. Schematic illustration of the optical spin pumping of resident electrons in QWs, resonant excitation to the exciton (X). Limit of high pump density.

Here τ_s^X is the electron-in-exciton spin relaxation time, τ_0^X is the exciton radiative lifetime, γ is a constant describing the efficiency of trion formation from an exciton, $T = T_+ + T_-$ is the total concentration of trions, and G_X is the exciton generation rate (σ^+ polarized pumping is assumed).

Solid lines in Fig. 3 show the spin of resident electrons as a function of the pump density calculated for various values of τ_s^X. Contrary to the case of trion resonant excitation, an initial increase of the net spin polarization is followed by its decrease to zero for very high pump densities [shown in panel (b)]. Qualitatively, such a behavior can be explained as follows. In the absence of electron spin relaxation, the formation of trions is prevented if the exciton concentration exceeds half of the electron concentration. However, the spin flip on an electron-in-exciton can provide the formation of trion even for higher exciton concentrations (schematically shown in Fig. 5). This is accompanied by a decrease of the net spin polarization of electrons [4]. At very high pumping densities, $G_X\tau_s/n_e \gg 1$, all resident electrons become bound to unpolarized trions and the system will consist of n_e unpolarized trions (no unbound electrons) and $X = G_X\tau_0^X$ excitons with the total electron-in-exciton spin $(X_+ - X_-)/2 = G_X\tau_0^X\tau_s^X/(\tau_0^X + \tau_s^X)$.

At low pump densities most of excitons form trions (the trion formation process can be considered as the fastest one when $\gamma n_e/2 \gg \tau_0^X, \tau_s^X$), which results in the spin polarization of resident electrons. At $G_X\tau_s/n_e \ll 1$,

$$S_z = -\frac{1}{2}G_X\tau_s. \tag{11}$$

and each absorbed photon participates in the trion formation either directly or via the exciton state. Therefore, the efficiency of the electron spin polarization is expected to be nearly independent of the pump energy. Comparing Eq. (11) and Eq. (7) one

can build a relation between the trion generation rate G entering Eq. (4) and exciton generation rate in Eq. (10) as $G_X = n_e G/2$. The spin polarization degree at high pump powers is predicted to be strongly dependent on the excitation energy and demonstrate qualitatively different behavior.

Pulsed excitation. In time-resolved experiments at low pump densities shortly after the pulsed optical excitation all excitons are bound to trions and the QW contains n_0^X trions (where $n_0^X = G_X \tau_{pulse}$ with τ_{pulse} being the pulse duration, $\tau_{pulse} \ll \tau_0^X$, is the number of photocreated excitons) and $n_e - n_0^X$ resident electrons with a total spin

$$|S_z| = n_0^X/2, \quad n_0^X \leq n_e/2. \tag{12}$$

As a result, n_0^X spins of resident electrons contribute to the Kerr rotation.

At higher excitation intensity ($n_0^X \geq n_e/2$) all $n_e/2$ resident electrons with $s_z = +1/2$ are bound to trions. Therefore, in absence of electron-in-exciton spin relaxation processes the trion density cannot exceed $n_e/2$, thus the total spin density of the electron gas is limited by $|S_z| < n_e/4$. The electron-in-exciton spin relaxation allows to convert the remaining $n_0^X - (n_e/2)$ excitons in trions. Obviously, the maximum number of formed trions cannot exceed the concentration of background electrons, n_e. The total spin of resident electrons after the excitons and trions have recombined can be estimated as (provided that the holes are unpolarized)

$$|S_z| \approx \frac{1}{4} \begin{cases} n_e - \frac{2n_0^X - n_e}{1+(2\tau_s^X/\tau_0^X)}, & \text{if } n_e > \frac{2n_0^X - n_e}{1+(2\tau_s^X/\tau_0^X)} \\ 0, & \text{otherwise.} \end{cases} \tag{13}$$

This equation is valid both for $B = 0$ and $B \neq 0$ when $n_0^X \geq n_e/2$, otherwise Eq. (12) holds. At $n_0^X = n_e/2$, the values of $|S_z|$ given by Eqs. (12) and (13) coincide and are equal to $n_e/4$. An initial linear increase of $|S_z|$ followed by a linear decrease is seen from Eq. (13). The decrease of initial electron spin as a function of pump intensity is steeper for smaller values of τ_s^X/τ_0^X, i.e. for shorter hole spin relaxation times. It is worth to stress that in this regime the electron spin polarization vanishes at very high pumping whereas, under resonant trion excitation, $|S_z|$ monotonously increases with increasing pump power and saturates at $n_e/4$.

2.2. Spin dynamics in transverse magnetic fields

Application of a transverse magnetic field (i.e., perpendicular to the initial spin direction) induces electron spin precession about the magnetic field, which is often called as spin beats. In general case time evolution of S_z is described by

$$S_z(t) \sim \mathrm{e}^{-t/T_2^*} \cos(\tilde{\Omega} t + \varphi) \tag{14}$$

where φ is an initial phase and T_2^* is the dephasing time of electron spin ensemble. The dephasing time is contributed by the coherence time of individual spins T_2 and by inhomogeneous spin relaxation time T_2^{inh} caused by, e.g., variation in electron g-factors: $1/T_2^* = 1/T_2 + 1/T_2^{inh}$ (see Chapter 6 in [2]). In the simplest case of isotropic and homogeneous system the spin relaxation of resident electrons is characterized by a single time constant $\tau_s = T_2$. In this case $T_2^* = \tau_s$, and the frequency of spin beats is equal to the Larmor frequency $\tilde{\Omega} = \omega_L$. In case of QWs experimental behavior appears to be somewhat more complicated for few reasons: (i) spin relaxation can be anisotropic [7], (ii) the main mechanism of spin dephasing can be caused by g-factor inhomogeneous distribution, (iii) the initial phase can depend on magnetic field.

2.2.1. Continuous wave excitation In many cases the regime of cw spin pumping in transverse magnetic fields (and the resultant Hanle effect) may be described in terms of the spin relaxation time τ_s. The corrections due to anisotropy and inhomogeneity of structures are discussed in subsection 2.2.2.

Trion resonant pumping. The system of kinetic equations describing spin dynamics of resident electrons and trions at low pump densities under trion resonant excitation has the following form [4]

$$\begin{aligned} \frac{dS_z}{dt} &= \omega_{\rm L} S_y - \frac{S_z}{\tau_s} + \frac{S_T}{\tau_0^T} - \frac{n_e}{4} G(t)\,, \\ \frac{dS_y}{dt} &= -\omega_{\rm L} S_z - \frac{S_y}{\tau_s}\,, \\ \frac{dS_T}{dt} &= -\frac{S_T}{\tau^T} + \frac{n_e}{4} G(t)\,. \end{aligned} \tag{15}$$

Here $S_T = (T_+ - T_-)/2$ is the effective spin density of the trions, S_y and S_z are the electron spin density components. Function $G(t)$ in Eq. (15) describes trion generation rate. It is assumed that z-axis coincides with the growth direction of the QW structure and the magnetic field is applied along x-axis. The solution for S_z, S_y and S_T in steady-state [$G(t)$ is a constant] readily writes

$$\begin{aligned} S_z &= -\frac{n_e}{4} G \frac{\tau_s \tau^T}{\tau_s^T} \frac{1}{1+(\omega_{\rm L}\tau_s)^2}, \\ S_y &= -S_z \omega_{\rm L} \tau_s \\ S_T &= \frac{n_e}{4} G \tau^T. \end{aligned} \tag{16}$$

Field dependence of S_z is described by the Lorentz curve, in agreement with Eq. (2). First line of Eq. (16) at $\omega_{\rm L} = 0$ agrees with Eq. (7). In the absence of trion spin relaxation ($\tau_s^T \to \infty$) application of an in-plane magnetic field does not result in steady-state spin polarization. This is in contrast with time-resolved experiments, where spin beats could be observed even for $\tau_s^T \to \infty$ (see Fig. 6 in Sec. 2.2.2 and Ref. [4]).

Typically, the trion spin relaxation time is much shorter than the electron spin relaxation time, $\tau_s^T \ll \tau_s$. Therefore, in moderate magnetic fields $\omega_{\rm L}\tau_s \sim 1$ the steady-state spin of electrons significantly exceeds the trion spin, $|S_z| \gg |S_T|$.

Exciton resonant pumping. In this case total spin of both resident electrons S_z and electrons in excitons $S_{Xz} = (X_+ - X_-)/2$ should be considered. Using Eqs. (10) in the rotating (with the frequency $\omega_{\rm L}$) frame of reference, one can derive the following equations describing the steady state spin of electrons and excitons in the weak pumping regime ($G_X \tau_s \ll 1$)

$$\begin{aligned} \boldsymbol{\omega}_{\rm L} \times \boldsymbol{S}_X - \frac{\boldsymbol{S}_X}{T_X} &= \frac{1}{2}\boldsymbol{G}_X, \\ \boldsymbol{\omega_L} \times \boldsymbol{S} - \frac{\boldsymbol{S}}{\tau_s} + \gamma \frac{n_e}{2} \boldsymbol{S}_X &= 0. \end{aligned} \tag{17}$$

Here $\boldsymbol{S}_X$ and $\boldsymbol{S}$ are the vectors of spin of electrons-in-excitons and of resident electrons, respectively, $\boldsymbol{G}_X$ is a vector directed along z-axis with an absolute value G_X and $T_X^{-1} = (\tau_0^X)^{-1} + (\tau_s^X)^{-1} + \gamma n_e/2$ is the inverse lifetime of electron-in-exciton spin.

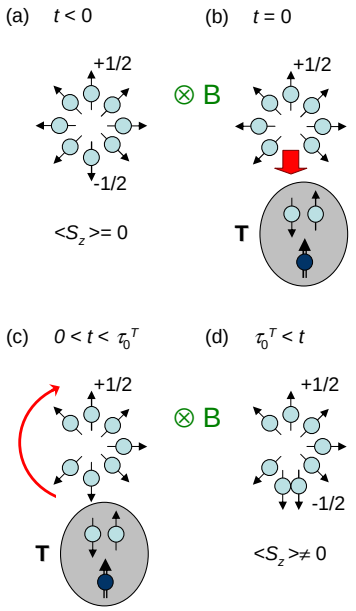

Figure 6. Scheme of generation of resident electron spin coherence in external magnetic fields via resonant photogeneration of trions. (a) Initial spin state of resident electrons which spin polarization in the plane perpendicular to the magnetic field is zero. Spins of resident electrons are precessing around B. (b) σ^- polarized photon generates a $(e, +1/2; hh, -3/2)$ electron-hole pair, which captures a $-1/2$ resident electron to form a trion. The resident electrons become polarized due to uncompensated $+1/2$ electron spin left. (c) During trion lifetime, τ_0^T, the net spin polarization precesses around the magnetic field. Trion state does not precess in magnetic field as on the one hand its electronic configuration is singlet and on the other hand in-plane hole g-factor is zero. (d) After trion recombination the $-1/2$ electron is returned (we neglect here spin relaxation of the hole in the trion). Final spin state of resident electrons with induced polarization is shown.

The solution of Eq. (17) for the z-component of spins reads

$$S_{Xz} = -\frac{1}{2}\frac{G_X T_X}{1+\omega_{\rm L}^2 T_X^2}, \qquad (18)$$
$$S_z = \frac{\gamma n_e \tau_s S_{Xz}}{2}\frac{1-\omega_{\rm L}^2 T_X \tau_s}{1+\omega_{\rm L}^2 \tau_s^2}.$$

At $\omega_{\rm L} = 0$ and $\gamma n_e/2 \gg 1/\tau_0^X, 1/\tau_s^X$ last line of Eq. (18) reduces to Eq. (11). Provided $T_X \ll \tau_s$ electron spin $S_z = S_z(\omega_{\rm L}=0)/(1+\omega_{\rm L}^2\tau_s^2)$, i.e. it is described by the standard Hanle curve [see Eq. (2)].

2.2.2. Pulsed excitation Spin quantum beats described by Eq. (14) are observed in direct time-resolved experiments under pulsed excitation. Here, we discuss the initial phase φ, the precession frequency $\tilde{\Omega}$ and the spin decay constant T_2^* entering Eq. (14) in detail.

Initial phase. The initial phase of spin beats in the case of trion resonant excitation strongly depends on magnetic fields. The reason is schematically illustrated in Fig. 6.

After pulsed excitation some of resident electrons with a certain spin projection are picked out to form trions. In the absence of hole spin relaxation the returning electrons after trion radiative recombination exactly compensate the generated spin of resident carriers. The transverse magnetic field breaks such a balance: the spins of electrons in trions do not precess while the spins of resident electrons rotate around the magnetic field, therefore the compensation is not complete. Detailed analysis shows that the electron spin as a function of time can be recast as [4]

$$S_z(t) = \frac{n_0^T}{2}[|1-\eta| \sin(\omega_{\rm L} t - \varphi) \mathrm{e}^{-t/\tau_s} - \eta' \mathrm{e}^{-t/\tau^T}], \tag{19}$$

where

$$\varphi = \arctan[(1-\eta')/\eta''], \tag{20}$$

η' and η'' are the real and imaginary parts of $\eta = (\tau_0^T)^{-1}/[(\tau^T)^{-1} - \tau_s^{-1} - \mathrm{i}\omega_{\rm L}]$. Hence, the initial phase is a non-monotonic function of the magnetic field.

Inhomogeneous distribution of electron g-factor. In order to take into account inhomogeneous broadening we assume that electron states are localized and characterized by a distribution of g-factors, $f(g)$. Hopping between different state is neglected, therefore it suffices to average the single electron spin precession $\exp(-t/\tau_s)\cos(\omega_{\rm L} t + \varphi)$ over this distribution. In the case of cw-pumping the Hanle curve, (16), should be averaged over $f(g)$ as well.

It is possible to obtain the analytical results when $f(g)$ is described by the Lorentzian function

$$f(g_e) = \frac{\sigma}{\pi[(g_e - g_0)^2 + \sigma^2]}, \tag{21}$$

where g_0 is the average value of g-factor and σ is the distribution width. Instead of (16) we have for $\langle S_z \rangle$

$$\langle S_z \rangle \sim \frac{1 + \sigma\mu_B B\tau_s/\hbar}{(1+\sigma\mu_B B\tau_s/\hbar)^2 + (g_0\mu_B B\tau_s/\hbar)^2}. \tag{22}$$

We note that Eq. (22) deviates from the standard Hanle curve in the magnetic fields B where $\sigma\mu_B B\tau_s/\hbar$ becomes of the order of unity. Typically, in QWs the g-factor spread is small, so that $\sigma \ll g_0$. As a result, inhomogeneous broadening does not strongly modify the Hanle curves in the region of $g_e\mu_B B\tau_s/\hbar \sim 1$.

The influence of inhomogeneous distribution of g-factors on spin beats is different. They can still be observed in high magnetic fields when $g_e\mu_B B\tau_s/\hbar \gg 1$. We obtain averaging with Eq. (21)

$$\langle S_z(t) \rangle \sim \exp(-\sigma\mu_B B t/\hbar - t/\tau_s)\cos(\omega_{\rm L} t + \varphi). \tag{23}$$

Comparison with Eq. (14) suggests that inhomogeneous broadening of the electron g-factor results in additional spin decay channel characterized by a time constant $T_2^{inh}(B) = (\sigma\mu_B B/\hbar)^{-1}$. In strong enough magnetic fields (provided $T_2^{inh}(B) \ll \tau_s$) this spin decay channel dominates spin beat dephasing process $T_2^* \approx T_2^{inh}$.

Anisotropy effects. In semiconductor quantum wells spin relaxation is known to be anisotropic, see Ref. [7] and references therein. In this case the inverse spin relaxation times are described by a tensor. In general case of an asymmetric quantum wells there are three linearly-independent components τ_{xx}, τ_{yy} and τ_{zz}, where $x \parallel [1\bar{1}0]$, $y \parallel [110]$ and $z \parallel [001]$. The spin relaxation times T_2 and the precession frequency $\tilde{\Omega}$ entering Eq. (14) are written then [8, 9]

$$\frac{1}{T_2} = \frac{1}{2}\left(\frac{1}{\tau_{zz}} + \frac{1}{\tau_{yy}}\right), \; \tilde{\Omega} = \sqrt{\omega_{\rm L}^2 - \frac{1}{4}\left(\frac{1}{\tau_{zz}} - \frac{1}{\tau_{yy}}\right)^2}. \tag{24}$$

Note, that the magnetic field is directed along x-axis. The Hanle effect is described by a Lorentzian ($\sim [1 + (\omega_{\rm L} T_H)^2]^{-1}$, where $T_H = \sqrt{\tau_{zz}\tau_{yy}}$) [7]. Thus, characteristic times τ_{yy} and τ_{zz} can be found

$$\tau_{zz} = \frac{T_H^2}{T_2} - \sqrt{\frac{T_H^4}{T_2^2} - T_H^2}, \tag{25}$$

$$\tau_{yy} = \frac{T_H^2}{T_2} + \sqrt{\frac{T_H^4}{T_2^2} - T_H^2}.$$

Here it is assumed that $\tau_{zz} < \tau_{yy}$, otherwise signs before square roots should be reversed. Rotating magnetic field in the QW plane allows to restore all components of the spin relaxation tensor.

2.2.3. Resonant spin amplification In time resolved experiments the periodic trains of laser pulses with repetition period of about $T_{\rm rep} = 12$ ns are commonly used. In case when the spin dephasing time is longer that $T_{\rm rep}$ the signal that does not fully decay from the previous pulse overlaps with the signal generated by the following pulse. Depending on the magnetic field strength it may cause constructive or destructive interference of these contributions, which complicates evaluation of the dephasing times. To overcome this complication the technique of the resonant spin amplification has been suggested [10].

In resonant spin amplification (RSA) experiments the magnetic field dependence of the electron spin is analyzed at a fixed pump-probe delay. If the pulse repetition period is commensurable with the spin precession in the magnetic field the spin polarization is enhanced because the spin injected in the system at the moments when the precessing spin of resident carriers is parallel to the spin of photocreated electrons.

The electron spin polarization can be written as

$$S_z(\Delta t) = \frac{s_0}{2}\, {\rm e}^{-(T_{\rm rep}+\Delta t)/T_2}\, \frac{{\rm e}^{T_{\rm rep}/T_2}\mathcal{C}[\tilde{\Omega}(T_{\rm rep}+\Delta t)] - \mathcal{C}(\tilde{\Omega}\Delta t)}{\cosh(T_{\rm rep}/T_2) - \cos(\tilde{\Omega} T_{\rm rep})}, \tag{26}$$

where $\Delta t \in [-T_{\rm rep}, 0)$ is the delay between the probe pulse and the following pump pulse,

$$\mathcal{C}(x) = \cos x - \frac{1}{2\tilde{\Omega}}\left(\frac{1}{\tau_{zz}} - \frac{1}{\tau_{yy}}\right)\sin x\,.$$

According to Eq. (26) and Fig. 7 the electron spin polarization represents a series of sharp peaks as a function of the magnetic field. These peaks correspond to the commensurability of the spin precession period and the pulse repetition period. The

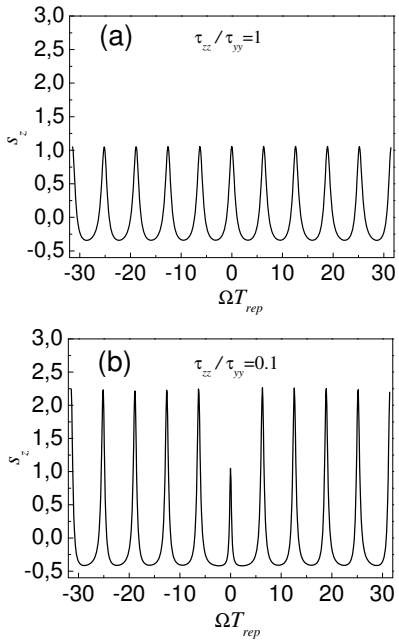

Figure 7. Kerr rotation signals calculated as a function of magnetic field at a constant pump-probe delay. Panel (a) shows the results in the case of isotropic spin relaxation ($\tau_{zz}/\tau_{yy} = 1$), and panel (b) corresponds to the strong anisotropy ($\tau_{zz}/\tau_{yy} = 1/10$. Signals are normalized by $s_z(B = 0)$. Other parameters are: $T_{\rm rep}/\tau_{zz} = 2/3$, $\Delta t/T_{\rm rep} = 1/250$. The details of calculations are given in Ref. [9].

analysis shows that the ratio of the zero field maximum to the next maxima (with not too large numbers $N \ll T_{\rm rep}/|\Delta t|$) is $\eta = (\mathrm{e}^{T_{\rm rep}/T_2} - 1)(\mathrm{e}^{T_{\rm rep}/\tau_{zz}} - 1)$ [9]. It equals to 1 in the case of isotropic spin relaxation, $\tau_{zz} = \tau_{yy}$, and smaller than 1 if $\tau_{zz} < \tau_{yy}$.

Inhomogeneous distribution of g-factor values can also affect the resonant spin amplification. As can be shown [9], the shape of zero-field peak is not affected by g-factor distribution. However, peaks with larger numbers become wider and smaller as the effective spin decay constant $T_2^* \approx T_2^{inh}(B)$ decreases with B [see Eq. (23)].

3. Experiment

3.1. Samples

We present characteristic experimental results based on two representative samples of CdTe/(Cd,Mg)Te QWs grown by molecular beam epitaxy on (001)-oriented GaAs substrates [11].

Sample #1 is a single 80-Å CdTe/$Cd_{0.7}Mg_{0.3}$Te QW [the PL spectrum is shown in Fig. 8(a)]. Free electrons in the QW are provided due to modulation doping by iodine donors in the $Cd_{0.7}Mg_{0.3}$Te barrier at a distance of 100 Å from the CdTe QW. An electron density in the QW of $n_e = 8 \times 10^{10}$ cm^{-2} was evaluated by optical means [12].

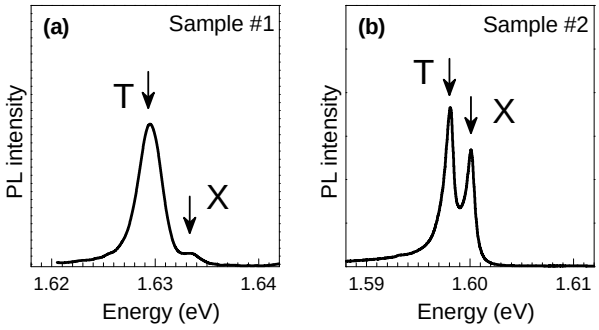

Figure 8. (a) PL spectrum of sample #1. (b) PL spectrum of sample #2. The arrows indicate the exciton (X) and trion (T) transitions. $T = 2$ K.

Sample #2 is a multiple quantum well (MQW) structure [the PL spectrum is shown in Fig. 8(b)]. It contains five 200-Å-wide CdTe QWs separated by 1100-Å-thick $Cd_{0.78}Mg_{0.22}Te$ barriers. The sample is nominally undoped. The low concentrations of electrons $n_e = 1.3 \times 10^{10}$ cm^{-2} in the CdTe QWs are due to residual n-type doping of barriers.

3.2. Experimental techniques

3.2.1. Continuous wave excitation For cw pumping, a tunable dye laser is used. Its radiation wavelength can be set in resonance with either the trion (T) or exciton (X) states (or one of some other high energy states) of a QW sample. The excitation is modulated between σ^+ and σ^- circular polarizations at a frequency of 50 kHz using a photoelastic quartz modulator. This allows to avoid nuclear spin contribution whose spin relaxation is much longer than the modulation period [1].

Hanle effect. The degree of circular polarization of the photoluminescence (PL) $P = (I_+^+ - I_+^-)/(I_+^+ + I_+^-)$ is detected by a Si-based avalanche photodiode and a two-channel photon counter. PL spectra are dispersed by a 1-m monochromator. The degree of circular polarization can be selectively detected on either the trion or exciton emission lines, denoted by P_T and P_X, respectively. When external magnetic field is applied in the QW plane P is suppressed to zero (Hanle effect). We note, the circular polarization in emission is sensitive to the polarizations of resident electrons (ρ_e) and excitons (ρ_X).

Two-color Hanle-MOKE. Alternatively, the net spin polarization of resident electrons can be probed by the magneto-optical Kerr effect (MOKE) [13, 14, 15]. In this experiment, one tunable dye laser is used for spin pumping and another tunable Ti:sapphire laser is used to probe spins. The latter is linearly polarized, and the photoinduced Kerr rotation θ is measured by a balanced diode detector and demodulated by a lock-in amplifier. Pump and probe energies (E_{pump} and E_{probe}) can be tuned independently, referred to as the two color mode [15]. By analogy with the Hanle effect, when external magnetic fields are applied in the QW plane θ is suppressed to zero. Also note, in the cw pumping regime concentrations of excitons and trions are much less than the concentration of resident electrons. Therefore, the

photoinduced Kerr rotation is proportional to the total spin of resident electrons only, $\theta \propto S_z$ (i.e., contributions from electrons in excitons and trions can be neglected).

3.2.2. Pulsed excitation Complementary, coherent spin dynamics can be studied by means of a time-resolved pump-probe Kerr rotation technique [2, 16]. It allows direct monitoring the evolution of the spin coherence of carriers generated by the pump pulses.

Time-resolved Kerr rotation (TRKR). A Ti:sapphire laser generates 1.5 ps pulses at a repetition frequency of 75.6 MHz. The spectral width of pulses is 1.5 meV allowing selectively excite different resonances in QWs. The laser beam is split in pump and probe beams (one color mode) and the time delay t between them is varied by a mechanical delay line. The pump beam is circular polarized by means of a photoelastic modulator operated at 50 kHz. The probe beam was linearly polarized, and the Kerr rotation θ is measured by a balanced photodetector. From an analysis of the decay of the Kerr amplitude $\theta(t)$ the spin dephasing time of electrons T_2^* can be extracted [17, 18]. And the precession frequency of $\theta(t)$ allows to determine the electron g-factor.

The TRKR technique can be further improved by using two synchronized Ti:sapphire lasers [4]. This allows to tune independently the pump and probe energies (two-color mode).

Note, for short delay times (in case of pulsed excitation) the concentration of photocreated excitons can be comparable with the concentration of resident electrons. Therefore, the Kerr signal is proportional to the total spin of electrons-in-excitons (S_X) and of resident electrons (S_z). This is in contrast to the cw Kerr signal, where contribution from excitons can be neglected.

Resonant spin amplification (RSA). It allows to measure T_2^* times in zero magnetic field limit [10, 17]. In this method an external magnetic field is scanned from small negative (−20 mT) to small positive fields (+20 mT) and a small negative time delay of the probe pulse is chosen ($\Delta t = -80$ ps). The RSA is very suitable for study of long living spin beats, when the Kerr signal has considerable amplitude at negative delays and interferes with the signal at positive delays.

3.3. Experimental results: Continuous wave excitation

3.3.1. Hanle effect. Typical photoluminescence (PL) spectrum of sample #1 is presented in Fig. 8(a). It consists of two lines separated by 3.8 meV. The high-energy line is attributed to the neutral exciton (X). The low-energy line originates from the negatively charged trion (T) [5], consisting of a hole and two electrons in the singlet state [19].

A Hanle curve detected on the exciton line (pump energy $E_{pump} = 1.648$ eV, $W = 2$ Wcm^{-2}) is shown in Fig. 9(a). It has two regions: (i) in the high-field region the polarization decreases slowly from 5.5% down to 3.5%, (ii) in the low-field region $|B| < 3$ mT a sharp peak is observed, where the polarization drops from ca. 6% down to 5.5%. The origin of the complex line shape of the Hanle curves in QWs has been qualitatively understood [20]. The point is that the trion is formed from the exciton and a resident electron $X + e \rightarrow T$, and this formation appears to be spin dependent.

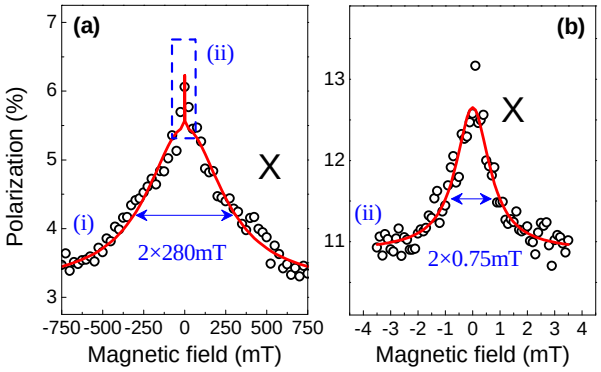

Figure 9. (a) A Hanle curve detected at the exciton (X) line of sample #1 ($E_{pump} = 1.648$ eV). $W = 2$ Wcm^{-2}. (b) The same rescaled for weaker magnetic fields. $W = 18$ Wcm^{-2}. Solid lines are fits to Eqs. (27) and (18). $T = 2$ K.

Hence, the degree of circular polarization detected on the exciton (P_X) and trion (P_T) emission lines can be written as [20]

$$P_X = \rho_X - \tilde{\gamma}\rho_e, \qquad (27)$$
$$P_T = P_X + \rho_e.$$

Here, $\rho_X \propto S_X + S_{X_h}$ and $\rho_e \propto S_z$ are spin polarizations of excitons and resident electrons, respectively, and $\tilde{\gamma}$ is a constant describing the efficiency of trion formation from an exciton. The total resident electron and electron-in-exciton spins (S_z and S_{Xz}) are introduced in Sec. 2.2.1. The total hole-in-exciton spin denoted by S_{X_h} results in incomplete depolarization of the exciton, as it is not affected by in-plane magnetic fields (in-plane hole g-factor is close to zero). Magnetic field dependencies of S_X and S_z are described by Eq. (18). In the limit $T_X \ll \tau_s$ depolarization of each of them follows the standard Hanle curve of Eq. (2) but with different characteristic magnetic field $B_{1/2}$.

The best fit to Eqs. (27) and (18) is shown by the solid line in Fig. 9(a). From this fit we find for region (i) $B^X_{1/2} = 280$ mT. It is ascribed to the depolarization of an electron within the exciton. Due to the electron-hole exchange interaction (enhanced within the exciton) the electron spin relaxation time τ_s^X shortens following the hole spin flips characterized by a time constant τ_{sh}. This provides in case of the strong electron-hole exchange interaction the width of the exciton Hanle curve $B^X_{1/2} = \sqrt{\tau_{sh}/\tau_0^X}\Delta_0/|g_e|\mu_B$, where Δ_0 is the electron-hole exchange splitting [21].

Regime (ii) in Fig. 9(a) is ascribed to the depolarization of resident electrons [20, 22]. It is measured with higher resolution for excitation density $W = 18$ Wcm^{-2} as presented in Fig. 9(b). Fitting to Eq. (2) (solid line) gives a characteristic magnetic field $B_{1/2} = 0.75$ mT. We find that $B_{1/2}$ depends on the excitation density in accord with Eq. (3) [22]. Extrapolation of $B_{1/2}$ to zero excitation density ($W \to 0$) allows to find the electron spin relaxation time $\tau_s = 19$ ns using the electron g-factor $|g_e| = 1.35$ (deduced from the spin beats as discussed is Sec. 3.4.1).

3.3.2. Two-color MOKE. We note that the contribution of the net spin polarization of resident electrons in the exciton or trion emission may be rather weak and difficult to detect. As an alternative, the two-color MOKE offers a highly sensitive technique.

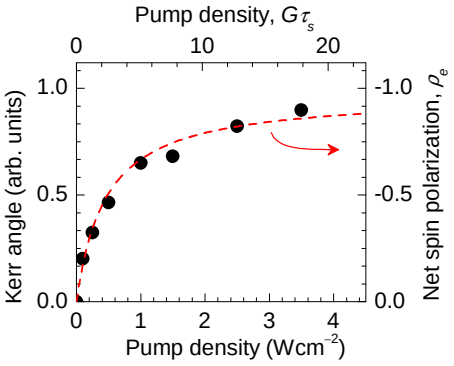

Figure 10. Normalized Kerr angle (proportional to the concentration of pumped electron spins) vs. excitation density for sample #2 (symbols). Pump (E_{pump} = 1.598 eV) and probe (E_{probe} = 1.597 eV) energies correspond to the trion resonance. Theoretical calculation of Eq. (5) is shown by the dashed curve. Fitting parameters are the same as in Fig. 3. $T = 2$ K.

We found that the Kerr angle obtained in cw regime is maximum when the pump energy coincides or slightly above and the probe energy is slightly below the X or T resonance [23]. Hence, independent tuning of pump and probe energies is an essential requirement for the two-color MOKE method. A typical dependence of the Kerr angle θ on the pump density W, obtained by this method in sample #2 is shown in Fig. 10 [23]. The pump (E_{pump} = 1.598 eV) and the probe (E_{probe} = 1.597 eV) energies relate to the trion resonance [PL spectrum of this sample is presented in Fig. 8(b)]. The concentration of pumped electron spins $S_z \propto \theta$ increases monotonically with W with a tendency to saturation for the pump densities exceeding 1 Wcm^{-2}. Theoretical calculation of Eq. (5) for the trion resonant pumping [presented in Fig. 3(a)] are shown by the dotted curve in Fig. 10. It follows quite well the experimental data.

Figure 11(b) demonstrates efficiency of spin pumping in sample #2 (E_{probe} = 1.597 eV) as a function of pump energy. Reflectivity (absorption) spectrum is presented in Fig. 11(a) for comparison. A pair of resonances associated with the neutral (heavy-hole) exciton (X) and negatively charged trion (T) is well resolved [5, 19]. Also several additional high-energy resonances are clearly seen in the reflectivity spectrum. Clear correlations in optical spectra of Fig. 11 are seen. At the low excitation density used ($W = 0.25$ Wcm^{-2}) the efficiency of spin pumping is nearly independent of whether the pumping is resonant with the heavy-hole exciton (E_{pump} = 1.600 eV) or the trion (E_{pump} = 1.598 eV), in accord with theoretical consideration in Sec. 2.1 [Eqs. (7) and (11)]. The net spin polarization of resident electrons changes its sign when pumping is resonant with the light-hole exciton (E_{pump} = 1.614 eV) as expected from the optical selection rules [1]. Remarkably, the spin pumping is still efficient without tendency to decrease for pump energies up to 50 meV above the bottom of the conduction band, when electrons with large kinetic energy are created [24].

Figure 12 shows the Hanle-MOKE curves for different probe energies while the pump energy is fixed at the exciton resonance, E_{pump} = 1.600 eV. These data are recorded at low excitation (pump density $W = 0.25$ Wcm^{-2}). When the probe energy is set slightly below the trion resonance E_{probe} = 1.597 eV the Hanle-MOKE curve is rather narrow [Fig. 12(a)]. From the best fit to Eq. (16) [see also Eq. (2)] we find

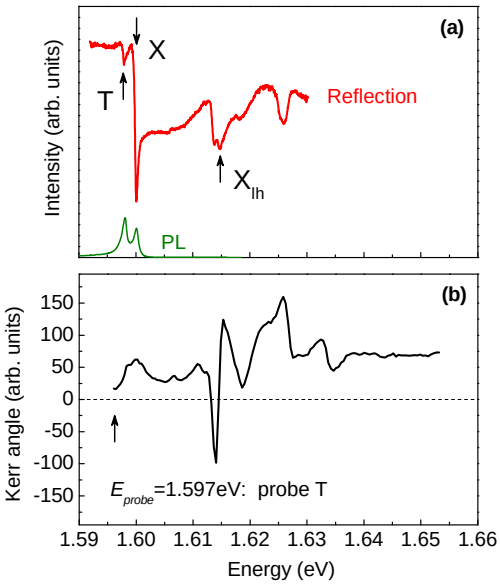

Figure 11. (a) PL and reflectivity spectra of sample #2. The trion (T), heavy-hole exciton (X) and light-hole exciton (X_{lh}) resonances in the QWs are indicated. (b) Spectrum of the spin pumping detected by means of the Kerr rotation at an energy of $E_{probe} = 1.597$ eV (slightly below the trion resonance). $W = 0.25$ Wcm^{-2}. $T = 2$ K.

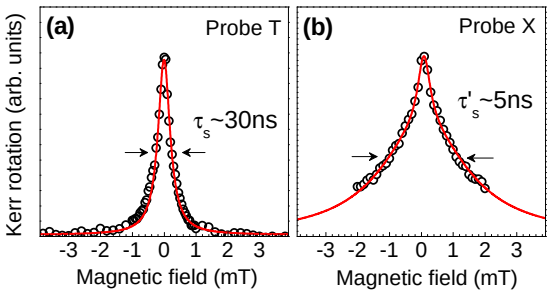

Figure 12. The Hanle-MOKE measured on sample #2 for different probe energies (a) $E_{probe} = 1.597$ eV (relates to the trion resonance) and (b) $E_{probe} = 1.599$ eV (relates to the exciton resonance). The pump energy is $E_{pump} = 1.600$ eV (the exciton resonance) in both cases. Solid lines are fits (see text for details). $W = 0.25$ Wcm^{-2}. $T = 2$ K.

$B_{1/2} = 0.23$ mT. With the electron g-factor $|g_e| = 1.64$ found in spin-flip Raman scattering experiments [25] or from spin beats (Sec 3.4.1), this characteristic field corresponds to the spin relaxation time of $\tau_s = 30$ ns. This value is in good agreement with the spin dephasing time $T_2^* = 30$ ns obtained in resonant spin amplification experiments for the same sample (as discussed in Sec 3.4.3).

When the probe energy is tuned to be slightly below the exciton resonance ($E_{probe} = 1.599$ eV), an additional contribution to the Hanle-MOKE curve appears [Fig. 12(b)]. We fit these data (solid line) by a sum of two Lorentz curves of Eq. (2) with different $B_{1/2}$ (dashed lines). Details of fitting procedure are discussed elsewhere

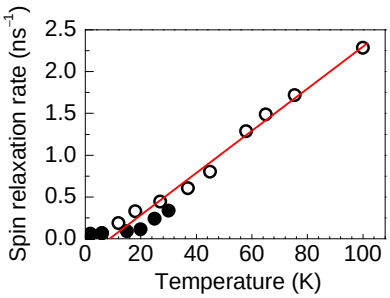

Figure 13. Temperature dependence of the spin relaxation rate obtained in cw experiments ($1/\tau_s$, solid symbols) and the spin dephasing rate obtained in pulsed experiments ($1/T_2^*$, open circles) measured for the pump resonant with the trion energy in sample #2. Line is a linear interpolation.

[23]. We find spin relaxation time of $\tau_s' = 5$ ns in addition to $\tau_s = 30$ ns. As the spin pump conditions are identical in both cases [i.e., Figs. 12(a) and (b)], the difference can be ascribed only to the selective sensitivity depending on the probe energy. A possible explanation originates from a spatially inhomogeneous distribution of resident electrons in the QW plane [26]. The trions being charged are more sensitive to the localization (for instance, in the electrostatic potential of ionized barrier donors) as compared to the neutral excitons. As a result, when the detection energy is set in resonance with the trion transition, mostly localized electrons are probed. Furthermore, the spin relaxation time of localized and free electrons may be different. Such an explanation is also confirmed by the temperature dependence of the spin relaxation time detected when the probe energy is in resonance with the trion state (solid symbols in Fig. 13). With increasing temperature localized electrons become delocalized, and as a consequence their spin relaxation rate $1/\tau_s$ rises. In Sec. 3.4.3 we compare these results with data obtained in TRKR experiments and discuss mechanisms of spin relaxation.

3.4. Experimental results: Pulsed excitation

We turn now to time-resolved experiments performed on the sample #2 by means of pump-probe Kerr rotation.

3.4.1. Time-resolved Kerr rotation (TRKR): One-color mode. Spin beats for different magnetic fields (pump and probe are set in resonance with the trion) in sample #2 are shown in Fig. 14. From fits to Eq. (14) one can find the spin dephasing time T_2^*, the precession frequency $\tilde{\Omega}$ and the initial phase φ. In case when anisotropy effects of Eq. (24) can be neglected (high magnetic fields) $\tilde{\Omega}$ is equal to the Larmor frequency $\omega_L = g_e \mu_B B/\hbar$ allowing to determine precisely the electron g-factor, $|g_e| = 1.64$. The spin dephasing time T_2^* decreases with magnetic field as $1/B$ (see inset) in accord with Eq. (23). Hence, in order to avoid the contribution of inhomogeneous distribution of g-factor values to the spin dephasing process, the spin quantum beats presented below are measured in the limit of low magnetic fields.

The initial phase φ depends on external magnetic field. The point is that the spins of the electrons forming a trion are in a singlet state and therefore do not precess around the magnetic field as the resident electrons do. Recombination of trions returns

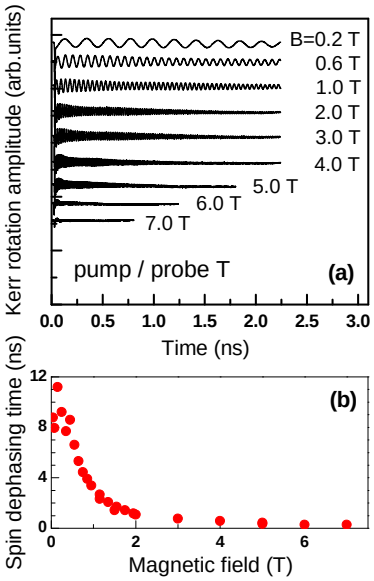

Figure 14. (a) Electron spin beats in pump-probe time-resolved Kerr rotation measures in sample #2 for different magnetic fields. Pump and probe are resonant with trion energy. (b) Evaluated spin dephasing time T_2^* vs. magnetic field. $T = 2$ K.

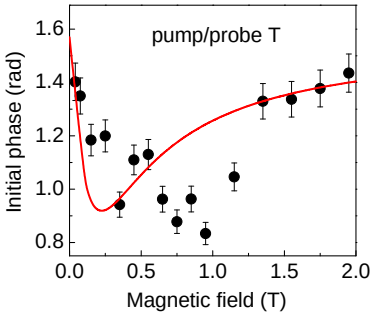

Figure 15. Initial phase of the Kerr rotation spin beats versus magnetic field for the degenerate pump-probe being resonant with the trion in sample #2. Pump density is 0.64 Wcm^{-2} and probe density is 0.5 Wcm^{-2}. The model calculation with $\tau_0^T = 30$ ps and $\tau_s^T = 60$ ps (solid line) is performed according to Eq. (20). $T = 2$ K.

partially z-polarized electrons to the 2DEG. Their spin orientation differs from that of the precessing electrons, which results in a shift of φ [4]. We have analyzed the initial phase by extrapolation the spin beats measured at longer delays back toward zero delay. The results are given in Fig. 15. A pronounced minimum is seen at $B \approx 0.7$ T in qualitative agreement with the model calculations shown by the solid line [Eq. (20)], performed with a trion lifetime $\tau_0^T = 30$ ps (obtained from the PL decay time [4]) and a spin relaxation time of the hole in a trion $\tau_s^T = 60$ ps (used as the only fitting parameter). We also assumed an electron spin dephasing time $T_2^* = 2$ ns (which corresponds to the experimental value at $B = 3$ T). The model demonstrates qualitative agreement with the experimental data.

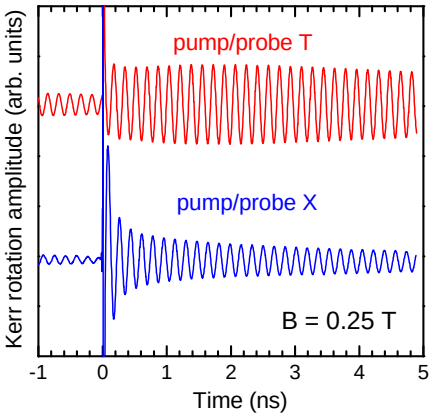

Figure 16. Kerr rotation measured by degenerate pump-probe being resonant either with the trion (upper curve) or the exciton (lower curve) energies in sample #2. Pump density is 1.5 Wcm^{-2} and probe density is 0.3 Wcm^{-2}. $T = 2$ K.

Time-resolved Kerr rotation signal measured for resonant pumping of either trion or exciton resonances is shown in Fig. 16, probe energy coincides with the pump one. Only long-lived spin beats of resident electrons are observed when the laser is resonant with the trion and two component decay is seen for the laser being resonant with the exciton. The experimental conditions (namely, low pump density 1.5 Wcm^{-2} and weak magnetic field $B = 0.25$ T) are chosen here to achieve longer electron spin coherence times [17, 4]. The delay time range between pump and probe in Fig. 16 covers 6 ns. Under these conditions the spin dephasing time of the resident electrons reaches 13.7 ns for pumping in the trion resonance and 4.2 ns for pumping in the exciton resonance. Moreover the spin coherence does not fully decay during the time interval of 13.2 ns between the pump pulses as is clearly seen by the beats at negative delays.

One can see also that the signal measured on the trion resonance contains only the long-lived spin beats of resident electrons. However the exciton signal clearly shows two component decay. The fast decay with a time of 50 ps is due to electron precession in photogenerated excitons. It disappears with the the radiative decay of excitons. The long-lived component with a time of 4.2 ns is due to the resident electrons, whose spin coherence is generated by excitons captured to trions shortly after photogeneration.

Theoretical analysis predicts qualitatively different dependencies of the Kerr rotation amplitude on excitation density for the excitons and trions [see Eqs. (9), (13)]. It is confirmed by experimental data from Fig. 17. Here the normalized values of the Kerr signals to their maximum values (which, according to our theoretical predictions, correspond to the electron spin density being equal to $n_e/4$) are shown. This allows us to compare the efficiency of spin coherence generation. One can see that in the low pumping regime the spin coherence generation efficiency per absorbed photon is practically the same for the laser tuned either to the exciton or the trion resonance. This is in a good agreement with cw experiments of Fig. 10 (see also discussion in Sec. 3.3.2) and the theory (Secs. 2.1.1 and 2.1.2): each absorbed photon creates a trion either directly or via an intermediate excitonic state, thus an electron with a given spin orientation is removed from the 2DEG. The strong pumping regime

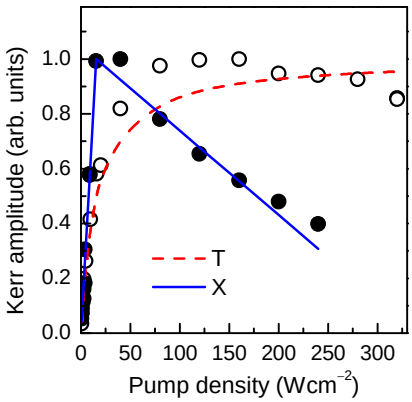

Figure 17. Normalized long-lived amplitude of the 2DEG Kerr rotation measured at a delay of 0.5 ns under resonant pumping of the excitons (closed circles) and the trions (open circles) in sample #2. Model calculations are shown by the lines. The dashed curve is calculated for trion resonant excitation according to Eq. (9). The solid lines are calculated for excitation at the exciton energy according to Eq. (13). In the latter case, the fitting parameter τ_s^X/τ_0 is found to be 10. $T = 2$ K.

is different for exciton and trion excitation. In the case of the laser tuned to the trion resonance the spin of the 2DEG saturates (the small decrease of the Kerr rotation amplitude can be attributed to heating of the 2DEG) while for the laser tuned to the exciton resonance a strong decrease of the spin coherence generation efficiency is seen.

The curves in Fig. 17 are the results of theoretical calculations based on the models outlined in Secs. 2.1.1 and 2.1.2. The dashed curve corresponds to trion resonant excitation, while the solid line is for exciton resonant excitation. For the dashed curve the only fitting parameter is the saturation level. For the solid line the only fitting parameter is the ratio between the electron-in-exciton spin relaxation time and the exciton radiative lifetime, which is $\tau_s^X/\tau_0^X = 10$. The spin relaxation of an electron in the exciton $\tau_s^X \sim 0.5$ ns appears to be shorter than that for the resident electrons. It has been shown that the electron-hole exchange interaction within the exciton provides an efficient spin decay channel in external magnetic field [21].

3.4.2. Time-resolved Kerr rotation (TRKR): Two-color mode. In QWs with low electron concentration (as for sample #2) the Fermi energy is smaller than the typical localization potential caused by well width fluctuations. As a result, at low temperatures a major fraction of electrons is localized. In order to have a deeper insight into the effects of electron localization on the spin coherence two-color pump-probe measurements have been performed in the regime where the longest dephasing times have been achieved, i.e. using a low pump density in a weak magnetic field of 0.25 T [4]. Figure 18 shows the results of such an experiment, where the pump beam is resonant with the exciton transition and the Kerr rotation signal is detected at either the trion or the exciton energy. As the excitation conditions are identical for both signals in Fig. 18, one would expect to detect the same dephasing times for the 2DEG, irrespective of the probe energy. Therefore, it is rather surprising to observe that the dephasing times of the electron coherence differ by a factor of two: $T_2^* = 10.8$ ns and 5.3 ns for probing at the trion and the exciton resonance, respectively.

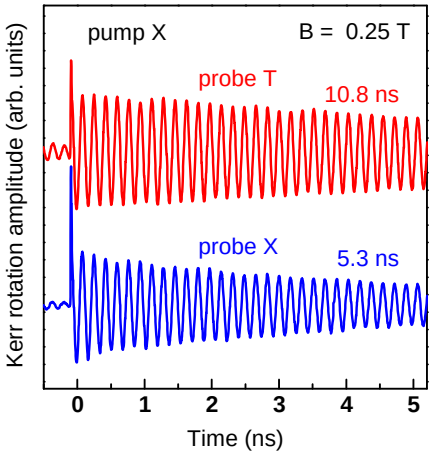

Figure 18. Kerr rotation measured by the two-color TRKR in sample #2. Probe is resonant with either the trion (upper curve) or the exciton (lower curve) energies. Pump is resonant with the exciton in both cases. Pump density is 1 Wcm^{-2} and probe density is 0.4 Wcm^{-2}. $T = 2$ K.

To explain this difference we suggest that different fractions of the resident electrons contribute to the Kerr rotation signal measured at the trion or the exciton energies. This can be understood if we take into account that different mechanisms lead to Kerr rotation signal at the exciton and trion energy. For detection at the trion resonance the effect is contributed by the variation of the trion oscillator strength, which is directly proportional to the concentration of electrons with a specific spin orientation [4, 12]. The trion stability (i.e., its oscillator strength) increases when resident electrons are localized in the QW plane [26], and these electrons possess a longer spin dephasing time. The Kerr rotation signal detected at the exciton energy monitors 2DEG spin beats mostly due to the spin-dependent exciton-electron scattering [27]. Possibility for this scattering to occur implies existence of free electrons. Therefore, at the exciton energy we address free or quasi-free resident electrons which have shorter spin dephasing times. This result is in good agreement with experimental data and conclusions drawn from the cw experiments of Fig. 12.

3.4.3. Resonant spin amplification. In certain magnetic fields the spins excited by the pulse train come in phase resulting in their amplification [10]. Such resonant spin amplification (RSA) in sample #2 presented in Fig. 19 was obtained for a small negative time delay of −80 ps between the probe and pump pulses. The spin dephasing time T_2^* time can be directly evaluated from the fit of RSA peak to Eq. (26) as it is shown in the inset. At a temperature of 2 K we evaluate $T_2^* = 30$ ns, which coincides with the spin relaxation time $\tau_s = 30$ ns obtained in cw Hanle-MOKE experiments (Sec. 3.3.2). To achieve such a long spin memory we reduce the pump density to the limit of 0.05 Wcm^{-2} where the signal has been still detectable.

A temperature increase causes broadening of the peaks, which reflects shortening of the spin dephasing time [18]. The similar behavior is observed when the pump density is increased at a fixed temperature of 2 K. Obviously the effect is related to the heating of the 2DEG and delocalization of electrons bound to QW width fluctuations. Free electrons have more channels for spin relaxation and therefore their spin coherence

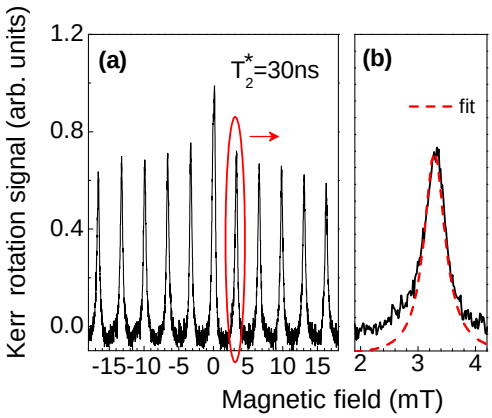

Figure 19. (a) Resonant spin amplification measured at a negative delay of -80 ps in sample #2. Pump density is 0.05 Wcm^{-2}. (b) The fit (dashed line) of a RSA peak to Eq. (26). Spin dephasing time of $T_2^* = 30$ ns is evaluated. $T = 2$ K.

decays faster.

Temperature dependence of the spin dephasing rate $1/T_2^*$ at $B = 0.25$ T is plotted in Fig. 13. Pump density of 0.8 Wcm^{-2} is chosen in order to follow the signal in the whole temperature range from $T = 2$ K to 100 K. The dephasing rate is about constant in the temperature range $T = 2 \div 7$ K and it increases linearly with a slope of 0.024 ns^{-1}K^{-1} up to $T = 100$ K. Characteristic depth of the electron localizing potential evaluated from the exciton linewidth in the PL is about 0.5 meV, which corresponds to an activation temperature of 6 K. For the temperature range from 7 K to 100 K the dependence $1/T_2^* \propto T$ holds with high accuracy. Such behavior is characteristic for the Dyakonov-Perel mechanism of spin relaxation. Theory gives the following expression for the spin relaxation rate [28, 29]:

$$\frac{1}{\tau_s} = \beta^2 \tau_p(T) k_B T. \tag{28}$$

Here τ_p is the momentum relaxation time and β is a coefficient characterizing dependence of the electron spin splitting on its wave vector. The effects of structure anisotropy on spin relaxation are neglected. The linear dependence measured experimentally allows us to suggest that in the studied sample τ_p is independent of temperature for $T < 100$ K. This is in agreement with the fact that the electron mobility in CdTe-based QWs is rather low (usually does not exceed few tens thousands Vcm^{2}s^{-1}) and τ_p is rather short and falls in the picosecond range.

4. Conclusions

With the use of various techniques based on continuous wave and pulsed excitation we have performed detailed experimental studies on optical spin pumping, spin relaxation and spin coherence of resident electrons in CdTe/(Cd,Mg)Te quantum wells. The experimental results are substantiated by a theoretical model based on classical approach to spins. Polarization of the resident electrons and generation of their spin coherence is provided by a capture of the resident electrons into trions. The trions in turn can be either photogenerated by resonant excitation or formed from the excitons.

Variation of pump energy (tuning to resonance with either the trion or the exciton) highlights details of the polarization process. Pump density dependencies for two excitation conditions are nearly the same for low densities (as each absorbed photon participates in spin pumping) and substantially different for high densities (for the trion pump the spin polarization tends to 100% while for the exciton pump the spin polarization decreases to zero). Spin beats and spin decay of resident electrons in external magnetic fields are shown to be subject of spin relaxation anisotropy and g-factor inhomogeneity. Independent variation of pump and probe energies proves that electron localization provides an increase of the spin relaxation time, as also confirmed by temperature dependent experiments. The spin relaxation time of localized electrons can achieve 30 ns, as independently found in continuous wave experiment in the limit of low pump density and in pulsed experiments by means of resonant spin amplification. Note, this is the longest spin relaxation time in QW heterostructures reported to date.

Acknowledgements

We acknowledge fruitful discussions with E. L. Ivchenko. Samples for these study have been grown in the Institute of Physics, Warsaw by G. Karczewski, T. Wojtowicz, and J. Kossut. This work was supported by the Deutsche Forschungsgemeinschaft (SPP1285 Spintronik via grants nos. YA65/5-1 and OS98/9-1 and by a grant no. 436 RUS113/958/0-1) as well as by the Russian Foundation for Basic Research. MMG was partially supported by the "Dynasty" foundation—ICFPM.

References

[1] *Optical Orientation*, edited by F. Meyer and B. P. Zakharchenya (North-Holland, Amsterdam, 1984).
[2] *Spin Physics in Semiconductors*, edited by M. I. Dyakonov (Springer-Verlag, Heidelberg, 2008).
[3] G. V. Astakhov and W. Ossau, *Phys. Status Solidi (c)* **4**, 3310 (2007).
[4] E. A. Zhukov, D. R. Yakovlev, M. Bayer, M. M. Glazov, E. L. Ivchenko, G. Karczewski, T. Wojtowicz, and J. Kossut, *Phys. Rev. B* **76**, 205310 (2007).
[5] K. Kheng, R. T. Cox, Y. M. d'Aubigné, F. Bassani, K. Saminadayar, and S. Tatarenko, *Phys. Rev. Lett.* **71**, 1752 (1993).
[6] G. V. Astakhov, D. R. Yakovlev, V. P. Kochereshko, W. Ossau, J. Nürnberger, W. Faschinger, and G. Landwehr, *Phys. Rev. B* **60**, 8485(R) (1999).
[7] N. S. Averkiev, L. E. Golub, A. S. Gurevich, V. P. Evtikhiev, V. P. Kochereshko, A. V. Platonov, A. S. Shkolnik, and Yu. P. Efimov, *Phys. Rev. B* **74**, 033305 (2006).
[8] V. K. Kalevich, B. P. Zakharchenya, K. V. Kavokin, A. V. Petrov, P. Le Jeune, X. Marie, D. Robart, T. Amand, J. Barrau, and M. Brousseau, *Phys. Solid State* **39**, 681 (1997).
[9] M. M. Glazov, E. L. Ivchenko, *Fiz. Tech. Poluprov.* **42** (8), 966 (2008) [Eng. transl. *Semiconductors* (2008), in press].
[10] J. M. Kikkawa and D. D. Awschalom, *Phys. Rev. Lett.* **80**, 4313 (1998).
[11] T. Wojtowicz, M. Kutrowski, G. Karczewski, and J. Kossut, *Acta Phys. Pol. A* **94** 199 (1998).
[12] G. V. Astakhov, V. P. Kochereshko, D. R. Yakovlev, W. Ossau, J. Nürnberger, W. Faschinger, G. Landwehr, T. Wojtowicz, G. Karczewski, and J. Kossut, *Phys. Rev. B* **65**, 115310 (2002).
[13] J. Stephens, J. Berezovsky, J. P. McGuire, L. J. Sham, A. C. Gossard, and D. D. Awschalom, *Phys. Rev. Lett.* **93**, 097602 (2004).
[14] S. A. Crooker and D. L. Smith, *Phys. Rev. Lett.* **94**, 236601 (2005).
[15] H. Hoffmann, G. V. Astakhov, T. Kiessling, W. Ossau, G. Karczewski, T. Wojtowicz, J. Kossut, and L. W. Molenkamp, *Phys. Rev. B* **74**, 073407 (2006).
[16] *Semiconductor Spintronics and Quantum Computation*, Eds. D. D. Awschalom, D. Loss and N. Samarth (Springer-Verlag, Berlin 2002).
[17] E. A. Zhukov, D. R. Yakovlev, M. Bayer, G. Karczewski, T. Wojtowicz, and J. Kossut, *Phys. Status Solidi (b)* **243**, 878 (2006).

[18] D. R. Yakovlev, E. A. Zhukov, M. Bayer, G. Karczewski, T. Wojtowicz, and J. Kossut, *Int. J. Modern Physics B* **21**, 1336 (2007).
[19] G. V. Astakhov, D. R. Yakovlev, V. V. Rudenkov, P. C. M. Christianen, T. Barrick, S. A. Crooker, A. B. Dzyubenko, W. Ossau, J. C. Maan, G. Karczewski, and T. Wojtowicz, *Phys. Rev. B* **71**, 201312(R) (2005).
[20] R. I. Dzhioev, V. L. Korenev, B. P. Zakharchenya, D. Gammon, A. S. Bracker, J. G. Tischler, and D. S. Katzer, *Phys. Rev.* Phys. *B* **66**, 153409 (2002).
[21] G. V. Astakhov, A. V. Koudinov, K. V. Kavokin, I. S. Gagis, Yu. G. Kusrayev, W. Ossau, and L. W. Molenkamp, *Phys. Rev. Lett.* **99**, 016601 (2007).
[22] G. V. Astakhov, T. Kiessling, D. R. Yakovlev, E. A. Zhukov, M. Bayer, W. Ossau, B. P. Zakharchenya, G. Karczewski, T. Wojtowicz, and J. Kossut, *Phys. Status Solidi (b)* **243**, 858 (2006).
[23] H. Hoffmann, G. V. Astakhov, T. Kiessling, W. Ossau, G. Karczewski, T. Wojtowicz, J. Kossut, and L. W. Molenkamp, *Phys. Rev. B* **74**, 073407 (2006).
[24] S. Pfalz, R. Winkler, T. Nowitzki, D. Reuter, A. D. Wieck, D. Hägele, and M. Oestreich, *Phys. Rev. B* **71**, 165305 (2005).
[25] A. A. Sirenko, T. Ruf, M. Cardona, D. R. Yakovlev, W. Ossau, A. Waag, and G. Landwehr, *Phys. Rev. B* **56**, 2114 (1997).
[26] G. Eytan, Y. Yayon, M. Rappaport, H. Shtrikman, and I. Bar-Joseph, *Phys. Rev. Lett.* **81**, 1666 (1998).
[27] G. V. Astakhov, V. P. Kochereshko, D. R. Yakovlev, W. Ossau, J. Nürnberger, W. Faschinger, and G. Landwehr, *Phys. Rev. B* **62**, 10345 (2000).
[28] M. I. Dyakonov and V. Yu. Kachorovski, *Sov. Phys. Semicond.* **20**, 110 (1986).
[29] E. L. Ivchenko, *Optical Spectroscopy of Semiconductor Nanostructures (Alpha Science*, Harrow, UK, 2005).